Chemical routes to materials

Morphology tuned plasmonic TiN nanostructures formed by angle-dependent sputtering process for SERS measurements

Tapan Barman[1], Libor Nozka[1,3,*], Vit Prochazka[4], Aleksandra Michałowska[2],
Sylwia Turczyniak-Surdacka[2], Radim Ctvrtlik[1,3], and Jan Krajczewski[2,*]

[1] *Faculty of Science, Joint Laboratory of Optics of Palacky University and Institute of Physics AS CR, Palacky University in Olomouc, 17. Listopadu 12, 771 46 Olomouc, Czech Republic*

[2] *Faculty of Chemistry, University of Warsaw, 02-093 Warsaw, Poland*

[3] *Joint Laboratory of Optics of Palacky University and Institute of Physics AS CR, Institute of Physics of the Czech Academy of Sciences, 17. Listopadu 50a, 772 07 Olomouc, Czech Republic*

[4] *Faculty of Science, Department of Experimental Physics, Palacky University, 17. Listopadu 1192/12, 771 46 Olomouc, Czech Republic*

ABSTRACT

Nowadays, most SERS platforms are based on plasmonic metals like silver and gold. The current scientific achievement is to construct SERS non-metallic platform with SERS activity not worse than in case of standard metallic platforms. The prominent combination of opto-electronic properties of TiN (titanium nitride) makes it a promising alternative plasmonic material for noble metals. So far, the TiN nanostructures are widely tested in catalysis, especially in photocatalysis. Despite the TiN potential in SERS sensing applications, there are still several fundamental issues preventing its wide practical application. In this work, the surface morphology of TiN layers was tuned from planar 2D to a high aspect ratio 1D nanorod-like structures by industrially scalable normal and glancing angle deposition (GLAD) pulsed DC reactive sputtering. The morphology of formed samples was studied by SEM microscopy, while the crystallographic properties were examined by Raman and XRD method. The opto-electrical parameters measured by spectroscopic ellipsometry, and DRS spectroscopy revealed substantial changes in optical properties of the TiN films with the variation of glancing angle. This in turn opened the way for tailoring the surface plasmon resonance and hence for SERS activity.

Springer

Introduction

For some specific applications, standard Raman scattering might not be considered as a very sensitive analytical method due to its very low cross section a few orders of magnitude lower than for absorption in IR and VIS region [1]. Such limitations could be overcome by the application of nanostructured plasmonic surfaces. Because the enhancement mechanism is related to surface such technique is the so-called SERS – Surface Enhanced Raman Scattering. So far, most of the SERS platforms are based on plasmonic metals like copper, silver, and gold [2, 3]. The special parameter called Surface-Enhanced Factor (SEF) allows for the comparison of various SERS platform activity. The EF determines the ratio of SERS signal to the normal Raman spectrum in the normalized for the same number of the analyte molecules. The development of novel SERS platform with improved properties allow to reach so high EF as even 10^7 [4, 5]. Therefore, SERS spectroscopy could be used for detection of even trace of organic molecules [6, 7], or even could be applied for single molecule detection [8, 9]. However, the topic of metallic-based SERS platform seems saturated, because their optical properties and the possibility of using them in SERS-based detection are practically fully utilized. The current challenge is to form a novel, highly active and stable SERS non-metallic plasmonic nanostructures, with SERS activity not worse than for standard metallic nanostructures.

In recent years, titanium nitride (TiN) has emerged as one of the most important alternative plasmonic materials due to its comparable plasmonic properties as that of gold and silver. Furthermore, titanium nitride possesses extraordinary thermal, chemical, and environmental stability while it is much cheaper as compared to its counterpart [10].

TiN has already been successfully applied as a novel plasmonic material in targeted drug delivery [11], cancer therapy [12], optical communication [13], for improving of efficiency of solar cells [14], artificial photosynthesis for production of solar driven fuel [15–17] and SERS for detecting ultralow amount of contaminants [18–22]. The plasmonic properties of nanomaterials vary depending on their size, shape, inter-particle distance, and surrounding dielectric media [23–26]. Therefore, for achieving specific plasmonic property, the nanomaterial fabrication must be tuned. For example, for applying TiN nanoparticles in the solar driven hydrogen production, the best performance is observed when the size of the nanoparticles is around 50 nm [27]. Similarly, TiN nano-pyramid with size of 20 nm and length 675 nm were found to greatly improve the efficiency of the solar cells [28]. For targeted drug delivery, TiN MXene nanostructured system was found to have impressive results [29]. Le Wang et al. recently reported enhanced SERS activity of core–shell Au-TiN nanoparticles of diameter 70 nm and interparticle distance of few nm [30].

Theoretical calculation proven than by experiments showed that the highest electromagnetic field occur in the gap between two plasmonic nanoparticles [31, 32] or on the edges and corners in case of non-spherical nanostructures [31, 33]. Therefore, the plasmonic coupling between two nanostructures can enhance the measured Raman signal by a factor even up to 10^{11} [34, 35]. To design a superior SERS substrate, controlling the inter-particle distance is one of the most important factors [36], while the most suitable nanoparticle distance of 1–5 nm is reported [37]. An array of TiN nanoparticle which may show remarkable plasmonic property in enhancing the efficiency of solar cell, photodetector, or photocatalytic may not at all be SERS active if the inter-particle separation is more than 20 nm [37]. Therefore, it is very important to study the role of surface nanostructure and inter-particle hotspot distance between the plasmonic nanostructures in a SERS substrate.

Plasmonic TiN nanostructures are basically synthesized by arc plasma discharge, chemical synthesis of TiO_2 followed by nitridation at high temperature in the presence of ammonia and by magnetron sputtering [38–40]. Among these techniques, a special rank belongs to a magnetron sputtering that is an industrially scalable and versatile technique for the fabrication of specially engineered TiN nanostructured thin films of controlled crystallinity, morphology, and stoichiometry on a broad range of substrates at room temperature [38]. In this respect, it is especially a glancing angle deposition (GLAD) and oblique angle deposition (OAD) where the substrate and sputtering source are tilted. This configuration has a direct impact on the sputtering flux getting deposited on the substrate where after a few monolayers a shadowing effect become the dominant growing effect under the conditions of sufficient glancing angle. As a result, the shadow regions prevent uniform distribution of sputtered species (atoms/ions) and provokes formation of pillar-like structures with dedicated large surface area and texture [41]. The geometrical aspects also have a

direct effect on the energy of the sputtered species reaching the substrate with a direct influence on the structural, optical and plasmonic properties of the films. So far, this method was mainly used for fabrication of Ag nanostructures with various geometry [42–44].

Yi-Jun Jen [18] has recently studied the formation of TiN nanostructured thin films by glancing angle deposition by reactive DC sputtering and compared their SERS activity for detection of R6G. Another similar approach was carried out by Nahid Kaisar [20] where they observed the effect of surface roughness of DC sputtered TiN thin film on the SERS activity of R6G at different concentrations. TiN nanostructures prepared by ion beam sputtering and reduction of TiO_2 nanotubes has been successfully applied as a SERS active substrate [45, 46]. It should be noted that one of the most crucial factors affecting the SERS activity is the controllable interparticle distance (generally any surface features like columns, pillars, spikes, etc.) in plasmonic nanostructure arrays. This opens new possibilities in hot-spot-engineering facilitating a strong local electromagnetic field enhancement which boosts SERS activity by several order of magnitudes. Strength of surface plasmon resonance hotspot generated between the TiN nanostructures enhances the SERS activity [47].

Despite the importance of the topic, there is still lack for a detailed study on the fabrication of SERS active substrate by tuning the glancing angle. Therefore, in this work, a detailed investigation on the tuneability of TiN nanostructures has been carried out at different glancing angles for the fabrication of superior SERS substrate.

Experimental methods

Samples preparation

TiN thin films were deposited from a 4″ Ti target (99.995% wt. purity) on soda-lime glass and Si (100) substrates (ultrasonically cleaned consecutively in acetone, ethanol, and deionized water for 5 min each and dried under N_2 flow) mounted on a rotating substrate holder, Fig. 1a. The samples were titled by an angle α with respect to the axis of the deposition beam as follows: 0° (a standard parallel-axes configuration), 45°, 67°, and 83°. The plasma reactor was pumped down to a base pressure of $1 \cdot 10^{-4}$ Pa by means of a turbomolecular pump in combination with a rotary pump. Sample deposition was then performed at a working pressure of 0.2 Pa in an Ar/N_2 background atmosphere (15 sccm/4 sccm, respectively) by a pulsed DC power supply at a frequency of 50 kHz with a duty cycle of 50%, power ~ 700 W, a discharge current of 1177–1099 mA, and a discharge voltage of 594–637 V for 10 min without any intentional substrate heating. The deposition rate was 20 nm/min or lower depending on the applied tilt α, Fig. 1b. Because of a lower sputtering rate, the film prepared for the angle of 83° was deposited for 30 min. Thicknesses of the TiN films ranged from 180 to 300 nm. For the narrative simplicity, the samples with TiN layers were labeled according to the angle of deposition α as follows: TiN 0°, TiN 45°, TiN 67°, and TiN 83°.
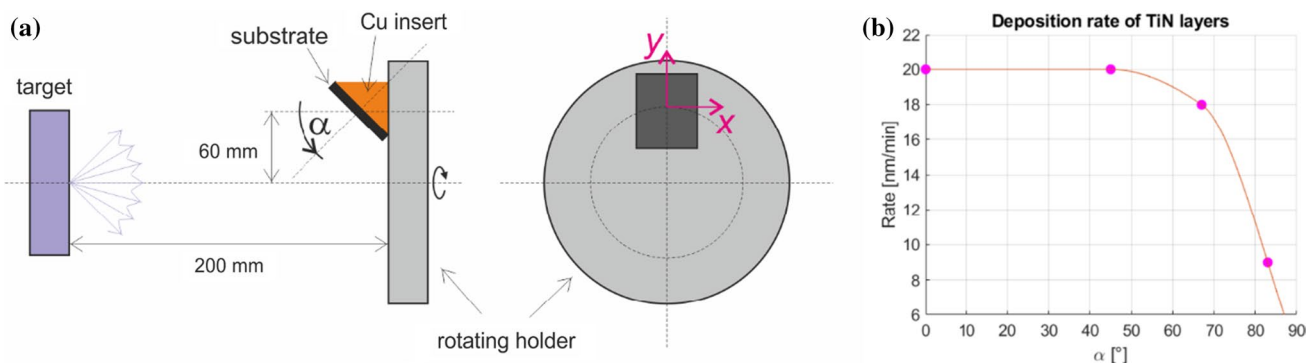

Figure 1 a Scheme of the deposition process by means of sputtering in a vacuum chamber, **b** deposition rate for the TiN films sputtered at different deposition angles.

Morphological, structural, and optical characterization

The surface and morphological properties of the TiN layers on Si were characterized using a Scanning electron microscopy (SEM) using a Merlin (Zeiss, Germany) field emission scanning electron microscope equipped with an energy-dispersive X-ray microanalysis (EDS) probe (Bruker). The thickness of TiN thin films (180 -300 nm) was measured via FIB-SEM and confocal microscopy. The crystalline structure of the TiN thin films was characterized by X-ray diffraction (XRD) measurements performed with a Bruker ADVANCE D8 diffractometer using the Co-Kα line emission (λ = 0.1789 nm). The measurement range used was 2ϑ = 20–100° in a grazing incident geometry using Soller slits with a resolution of 0.4° and a step size of 0.05°. The incident angle ω was 3°. The identification of crystalline phases was performed with the Diffraction Eva software (BRUKER) in conjunction with Crystallographic open database [http://www.crystallography.net/cod/]. Diffraction patterns were acquired on samples grown on glass substrates to avoid the contribution of Si peaks after checking that the same results were achieved for samples grown on Si substrates. The optical properties of the TiN layers on Si substrates were investigated by spectroscopic ellipsometry with a J. A. Woollam M2000-D UV/VIS variable-angle spectroscopic ellipsometer (VASE) in the spectral range from 190 to 1000 nm at angles of incidence from 55 to 75° with a step of 5°.

SERS Spectroscopy

The Raman reporter molecule was the Nile Blue purchased from Sigma-Aldrich. The water was purified by a Millipore Milli-Q system and had a of ca. 18 MΩ/cm. Raman spectra were collected using a Horiba Jobin – Yvon Labram HR800 spectrometer equipped with a 600-grooves/mm holographic grating and a Peltier-cooled CCD detector (1024 × 256 pixel). An Olympus BX40 optical microscope equipped with 50 × long distance objective was connected to the Raman spectrometer. Excitation radiation with the wavelength of 632.8 nm was provided by a He – Ne laser. The excited surface area in the experiments with 50 × objective was approximately 1.1 μm^2.

Results and discussion

Morphology and microstructure of the films

Figure 2 shows a plan-view of the TiN thin films. The film morphology showed a well-developed columnar growth typical for sputtered TiN films. A columnar structure was observed for the film deposited at the zero tilt (TiN 0°), while a columnar pillar structure with increasing degree of porosity/voids was observed for the films sputtered at the titled cases. For the normal incidence, the sample TiN 0° exhibited a dense homogeneous character with small grains. As the deposition angle α increased, the surface morphology gradually changed to an oriented one with a direction dictated by the atomic shadowing effect. Typical triangular facets of grains, representing the (111) direction,
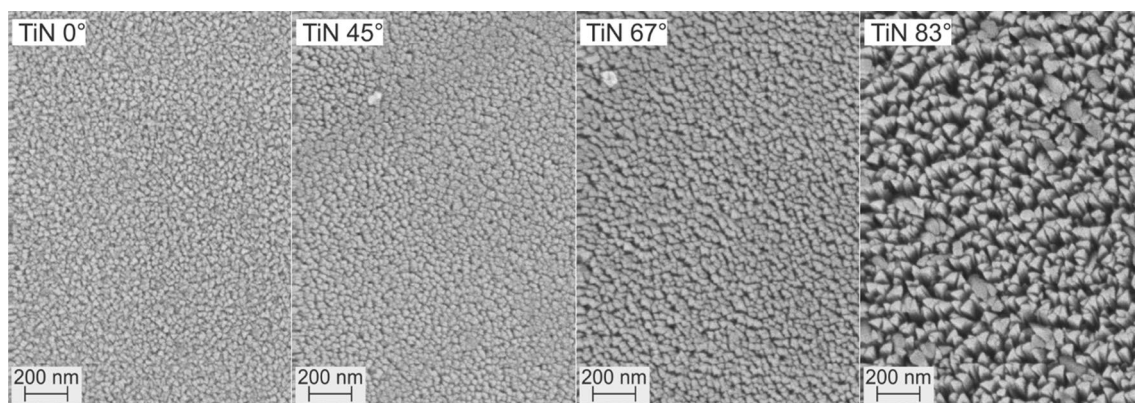

Figure 2 SEM plan-view images of deposited TiN layers (mag 100000x).

can be clearly distinguished on the top of the films, while the grains sizes increased with the substrate tilt. This was especially evident for the columnar pillars grown at the tilt angle of 83°, Fig. 3.

XRD patterns for the as-deposited TiN films are presented in Fig. 4a. Samples were positioned so that the x axis of the sample lied in the incidence plane of the diffractometer (given by wave vector of incident and scattered radiation), see also Fig. 1a. The presence of (111), (200), (220), and (311) characteristic x-ray diffraction peaks in all the samples confirmed the formation of thin TiN films. The peak of the (200) diffraction plane diminishes as the tilt α of the deposition grows. This is caused by a strong preferred orientation of the film grown on the highly tilted substrates (67° and 83°).

Orientation of the seeds in the growing layer was investigated by searching the inclination angle β of the diffraction plane 200 with respect to the surface plane. The inclination angle was obtained from position of the maximal intensity scattered from the sample with respect to the angles ψ and ϕ of Euler cradle rotation according to the following formula: $\beta = \omega + \psi - \theta$, where $\omega = 3.0°$ was the incidence angle of x-ray and $\theta = 25.1°$. Figure 4b shows how the inclination angle β changed with the samples tilt angle α for the diffraction plane (200).

Optical properties

Ellipsometry

Detailed opto-electrical properties of the TiN layers deposited on Si substrates were studied by the variable angle spectroscopic ellipsometry (VASE) in UV and VIS spectral regions. An eventual effect of the Si substrates on the ellipsometry measurements was neglected due to the metallic nature of the TiN films in these wavelength regions and their thickness above
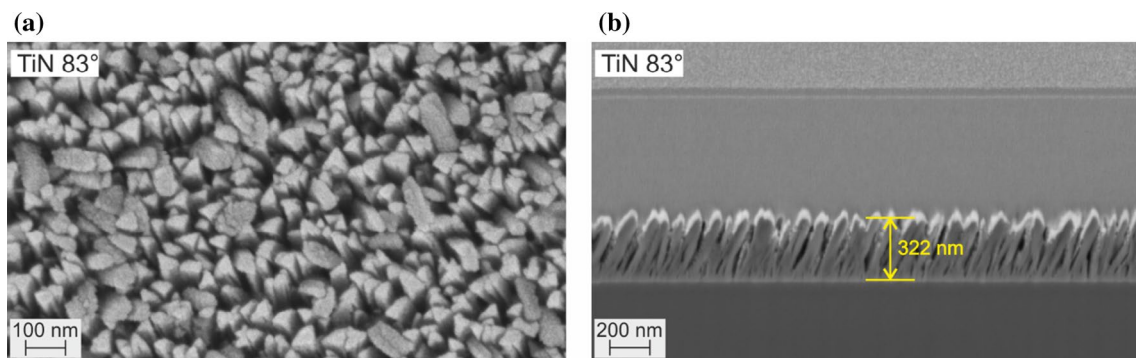

Figure 3 Detailed SEM images of TiN 83°: **a** plan-view under a magnification of 200,000, **b** a cross section view of columnar structure of a thickness of 322 nm.
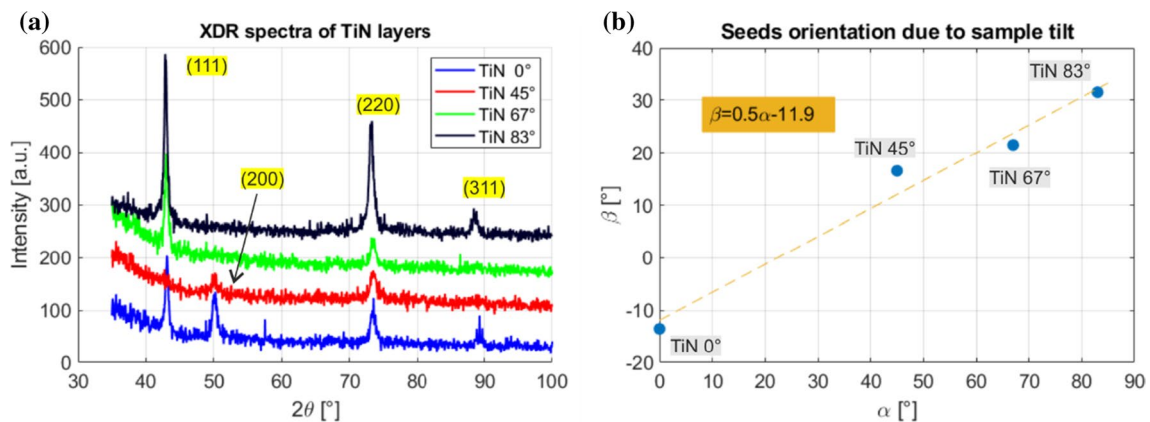

Figure 4 **a** XRD spectra of TiN samples ($\phi = 0°$), **b** inclination angle of seeds with respect to the surface plane of samples as a function of introduced tilt of samples during the sputtering process.

80 nm. Except TiN 0°, optical responses of the samples were not isotropic due to the introduced tilt of the samples with respect to the axis of the deposition. Thus, this anisotropy was related to the morphology of the layers. The samples were measured in two directions: along the axes x and y, see Fig. 1a. Results by ellipsometry are presented in Fig. 5 for both directions in form of the dielectric function $\varepsilon = \varepsilon_1 + i\varepsilon_2$.

Concerning x direction, all samples except the TiN 83° showed optical responses with a typical shape for metals: rapid drop of ε_1 at longer wavelengths (here in red VIS and near IR regions) accompanied by increase of ε_2 which follow the Drude model for metals. The wavelength at which ε_1 reaches the zero is called the screened plasma wavelength. On the other hand, the optical response of the TiN 83° sample was fully dielectric (ε_1 remained above zero) although the material TiN itself is a metal. The metallic behavior was less and less pronounced as the tilt angle α increased. There was a peak of ε_1 around 400 nm for the samples sputtered at 0°, 45°, and 67°. This was attributed to the resonant oscillation for electric polarization which corresponds to dielectric response of samples in this (UV) wavelength region (where $\varepsilon_1 > 0$ in general).

As far as the y direction, only the sample TiN 0° kept the same metallic optical response as in the case of the x direction. The others exhibited pure dielectric responses in the measured spectral region including red VIS and near IR. This implied that a preferential columnar growth of the layer seeds imposed by tilting of samples led to directionally dependent optical response of the layers in the VIS and NEAR. Dielectric behavior of the optical response could be attributed to locking of free electrons if TiN material in columnar structures, especially in the y direction. Such electrons could not effectively screen out imposing light beam causing a suppression of metallic response and revealing a dielectric one.

The SERS activity is inherently related to the existence of surface plasmon-polaritons (SPPs) [47]. We kindly refer the reader to our previous work [10] in which plasmonic properties of our TiN layers deposited at normal angle ($\alpha=0°$) were already discussed. The SPPs (either localized or propagating) arise in a medium with free-carriers for which $\varepsilon_1 < 0$ depending on the wavelength of impacting light. Otherwise the electromagnetic modes are in the form of Brewster (radiation) modes. The ε_2 defines the length of propagation of SPPs either in the surface plane (L_{SPP}) of inward the layer (L_{2z}) or outside to the ambient medium (L_{1z}) [10, 47].

Subsequent analysis of plasmonic properties of sputtered TiN material was restricted to the sample TiN 0° which exhibited, as the only one, the isotropic optical response. The others exhibited strong influence of the surface morphology preventing analysis of dielectric function of the material itself. Results are summarized in Fig. 6. SPPs modes existed above 519 nm (where $\varepsilon_1 > 0$) and were lossy in the VIS region (visually depicted by width of the surrounding red or blue zones for given modes). The propagation lengths for all defined directions are compared in Fig. 6b. The propagation length L_{2z} to the TiN layer (penetration) was 23 nm at 633 nm (the working wavelength of the SERS spectrometer) and the L_{1z} (toward the ambient air) was 151 nm. The SPPs were therefore truly trapped on the surface.
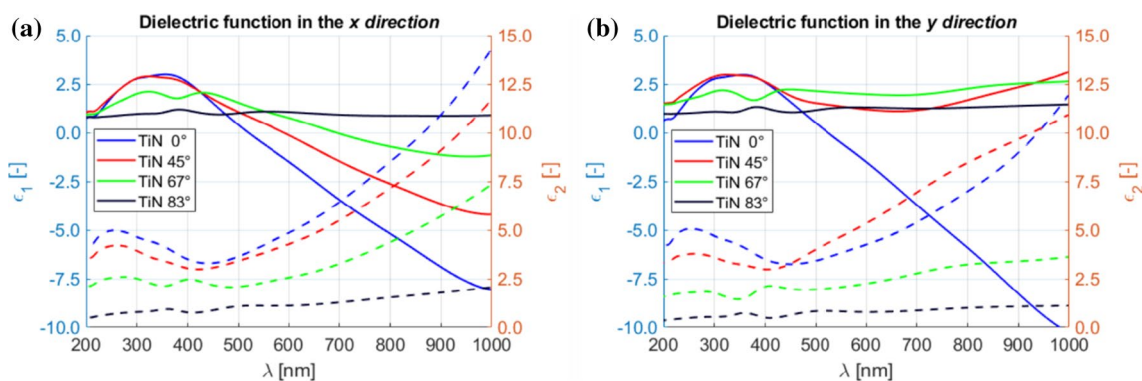

Figure 5 Dielectric function of samples TiN measured in **a** x direction and **b** y direction according to the scheme in Fig. 1a.
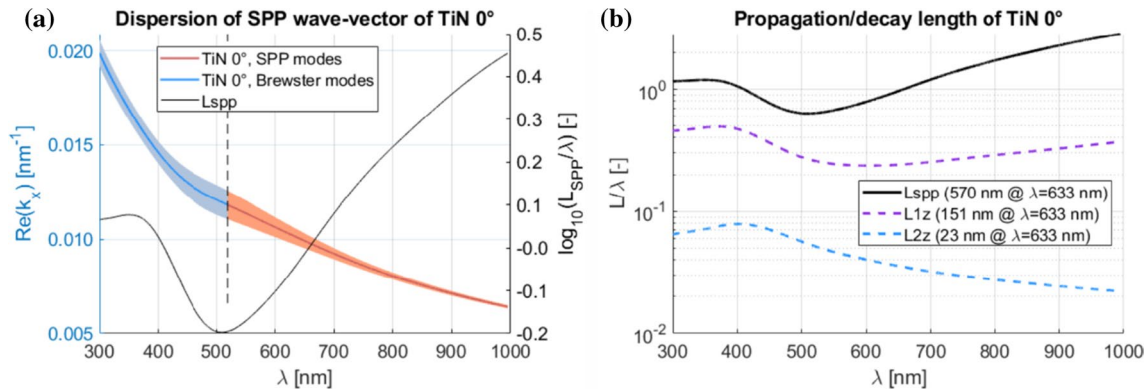
Figure 6 Results of basic plasmon analysis of the sample TiN 0°: **a** dispersion of wave-vector of surface plasmon-polaritons (SPPs) including length Lspp of their propagation in the plane of the surface, **b** length of propagation Lspp together with propagation lengths of SPPs inward the layer (L2z) and outside to the ambient air medium (L1z).

Absorbance in UV/VIS spectral regions

Figure 7a shows the UV/VIS response of the samples by means of the diffuse reflectance spectroscopy (DRS) technique. The DRS spectra were recorded in the range of 200–800 nm. As one can expect, all samples exhibited a broad peak in the visible region with the maximum located between 400 and 500 nm. The spectrum widening and small peaks located below 400 nm correspond to the band gap of TiN and has a good relationship with the literature [48]. The SPR peak road and located in the region from 400 to even 700 nm. The spectra are shifted vertically for more clarity. The half-width of the SPR peak could be related to the size dispersity of plasmonic nanostructures. Therefore, one can assume that the TiN 45° sample exhibited the highest homogeneity of formed nanostructures. The rest of the spectra had a bit widened SPR peak indicating on significantly lower homogeneity of the size and shape of formed nanostructures.

Raman spectra of TiN films

Raman spectra for 4TiN samples are shown in Fig. 7b. Regardless the tilt, all the layers exhibited the same character of the spectrum containing broad bands around 540, 840, and 1040 cm^{-1}. The low-frequency band below 300 cm^{-1} was caused by acoustical phonons, while the peaks at 550 cm^{-1} corresponded to the optical phonons [49]. It is well known that peak shift to higher frequencies indicates lower nitrogen concentrations and hence the formation of non-stoichiometric TiN_x [50]. Therefore, the recorded Raman spectra can
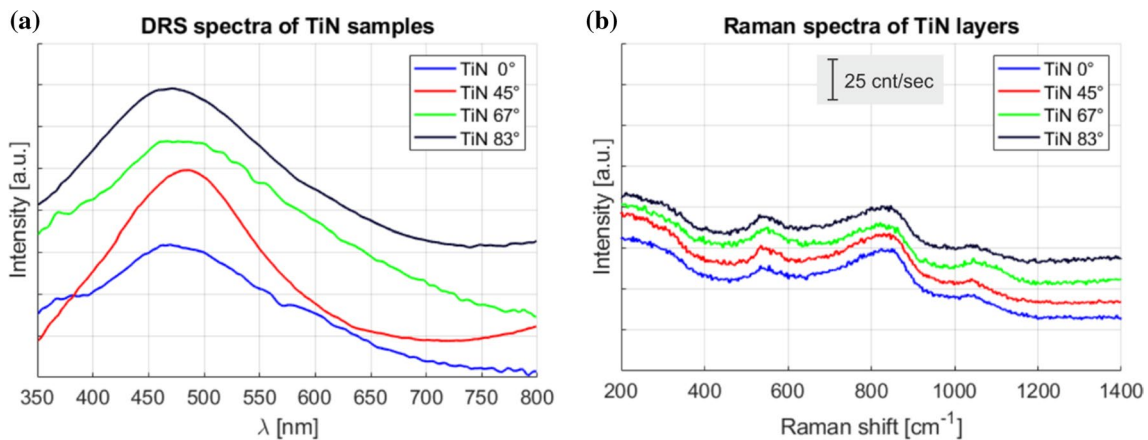

Figure 7 **a** Absorbance of TiN samples measured by DRS method, **b** Raman spectra of the samples measured at 633 nm.

therefore be easily associated with fully stoichiometric TiN structures.

Model SERS measurements

Due to the fact that the TiN material exhibited plasmonic properties, the TiN samples were tested as SERS platforms for a model analyte detection. Typically, dyes or thiolated organic molecules are used as a Raman reporter molecule. The thiol group (-SH) exhibits a very high affinity to the metal surface. As an effect, a strong covalent bond M-S (M = Au, Ag, Cu) is created [51]. Therefore, the whole active surface could be covered by a monolayer of thiolated target molecules. However, the surface chemistry of semiconducting TiN surface is different than those of typical for metals and thiolated molecules do not exhibit almost any affinity to non-metallic TiN nanostructures. Therefore, dye Nile Blue was used in this work as a common model analyte for SERS measurements. Based on ellipsometry results, a red excitation beam with a length of 633 nm and a 50 × long distance objective was used for maximum Raman signal amplification.

The dye, precisely Nile blue (NB), was used as the model molecule to examine the activity of prepared TiN samples for the SERS applications. The samples for SERS tests were prepared by dropping 7 µl of the solution of the appropriate concentration (from 10^{-4} to 10^{-6} M) of Nile blue on the TiN surface of the samples. The obtained results were averaged from 30 measurements. The SERS spectra of Nile blue recorded on the samples are presented in Fig. 8. The most visible band occurred at 592 cm^{-1}, which was assigned to C–C–C and C–N–C deformations [52, 53]. The other modes characteristic for the NB molecules also appeared in the spectrum in accordance with previous studies [52, 54]. All samples allowed for recording vibration spectra of the dye with a good signal-to-noise ratio. In the case of the TiN 45° sample, it was possible to detect a concentration of 10^{-6} M in solution of the Nile blue, Fig. 8b. Interestingly, the dye molecules could not be easily removed from the TiN surface by water rinsing (even by washing with any other organic solvent). This fact resulted from the small size of TiN nanostructures and as an effect of trapping dye molecules in the nanopores of the layers. This fact prevents the reversibility of the proposed TiN SERS platform.
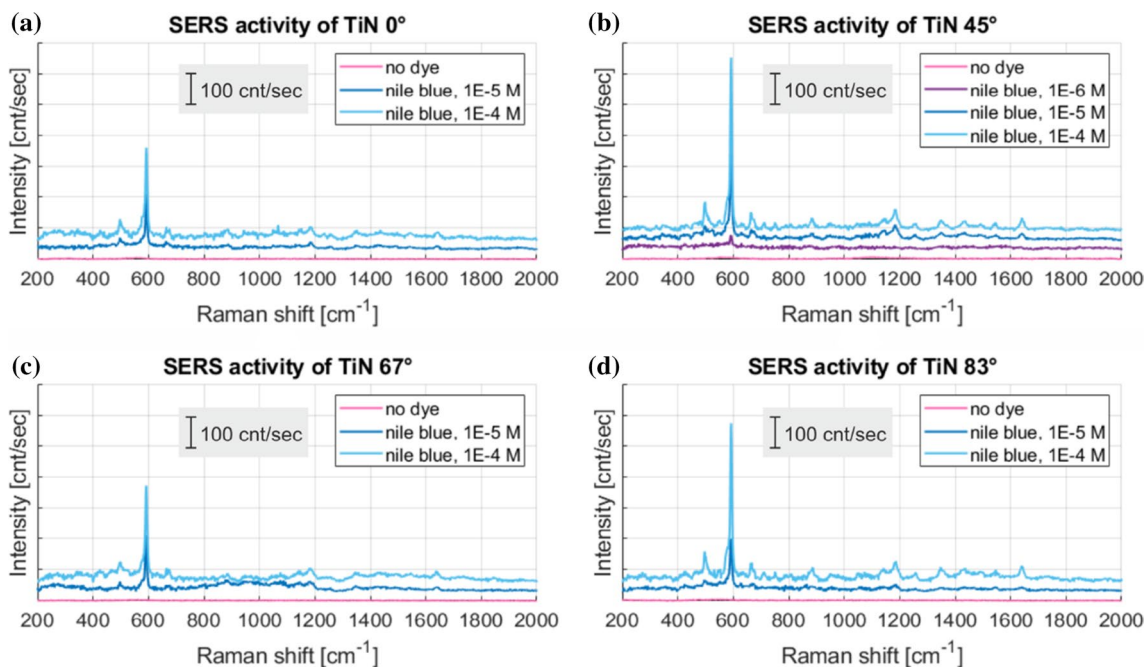

Figure 8 SERS spectra of a Nile blue reporter on **a** TiN 0°, **b** TiN 45°, **c** TiN 67°, and **d** TiN 83° samples for various concentrations of the reporter dye. Only the TiN 45° exhibited a SERS activity for the concentration of 1E-6 M of the dye.

Discussion

The aim of this work was to prepare SERS active structures with TiN layers of nanostructured morphologies tuned by introduced tilt of samples during the sputtering process of the TiN films. A closer look on SEM pictures revealed a columnar structure of deposited TiN grains whose columns size, shape, and density varied with the tilt. Optical responses of the layers measured by ellipsometry exhibited directional dependency driven by the applied tilt in the given configuration according to Fig. 1a. The response of TiN material is of metallic character under normal deposition conditions (0°). As the tilt α grows, the metallic character of the optical response is weaker in the direction tangential to the rotation (axis x in Fig. 1a) and it became dielectric at 83°. We assume this is related with decrease in the mean free path of free electrons in the layer due to texture of dimension in order of tens of nanometers in that direction. On the other hand, there is no metallic character in the direction perpendicular to the rotation (axis y in Fig. 1b) for any tilt except 0° (whose response is isotropic). It does not mean the TiN layers are not plasmonic. TiN is intrinsically metal, but its deposited columnar grains effectively localize free (valence) electrons suppressing metallic behavior in larger scales (in order of hundreds of nanometers in case of the used ellipsometry). And of course, the grains allow for arising of localized plasmon resonances which makes SERS effect possible in this case.

As shown in Fig. 8, the samples produced under the tilts of 45° and 83° exhibited recognizably higher SERS activity against Nile blue reporter compared to the others. Moreover, only the sample TiN 83° exhibited SERS activity for concentration down to 10^{-6} M of the dye. However, the SERS activity is weaker when compared other published results. The reason obviously lies in the overall morphology of created nanostructures. Grains do not exhibit sharp edges, for example like pyramids [10]. Sharp edges and apexes of nanostructures create hot-spots in terms of local field intensity enhancement factor (LFIEF) which quantitatively describe the SERS in frame of the electrostatic approximation approach. In the case of presented TiN nanostructures, a mean LFIEF is lower than one for mentioned pyramids.

On the other hand, presented sputtering method is a simple mean of production of functional nanostructures and there is still room for improving by means of optimization of sputtering process.

Conclusion

In this work, we proposed a novel method of deposition of TiN nanostructured layers in order to tune size, shape, and density of TiN grains in the form of columnar structures. The TiN layers were deposited by means of a pulsed DC magnetron sputtering process in the glancing angle setup. The crystallographic characterization confirmed formation of fully stoichiometric TiN nanostructures. It was found that SERS activity depended on the angle of the sputtering deposition (introduced tilt). The highest SERS activity was found for the samples deposited by the tilt angle of 45°. The lowest concentrations of dye still possible to detection was evaluated to the order of 10–6 M. This means that the TiN material can be successfully used in the SERS applications. However, due to the fact of small dimensions of formed nanostructures during the sputtering deposition (few nanometers up to 10 nm), the SERS activity is not strong when compared to other literature reports. Like other metal-based SERS platforms, TiN nanostructures must be carefully planned and prepared in order to obtain nanostructures with high SERS activity.

Author contributions

TB helped in initial idea, sputtering of TiN, and paper editing. LN performed ellipsometry measurements and analysis and paper editing. VP: XRD done measurements and analysis. STS analyze structural characterization, SEM and DRS done measurements. JK performed idea of research, SERS done measurements, data analysis, and paper writing. AM: SERS done measurements, data analysis, and paper writing. RC: optimization of TiN sputtering and sputtering.

Data availability

All data can be made available to interest readers upon request.

Declarations

Conflict of interest   The authors declare no conflict of interest for the research presented.here.

References

[1] Petry R, Schmitt M, Popp J (2003) Raman spectroscopy-a prospective tool in the life sciences. ChemPhysChem 4:14–30. https://doi.org/10.1002/cphc.200390004

[2] Kelly KL, Coronado E, Zhao LL, Schatz GC (2003) The optical properties of metal nanoparticles: the influence of size, shape, and dielectric environment. J Phys Chem B 107:668–677. https://doi.org/10.1021/jp026731y

[3] de Santos E B, Sigoli FA, Mazali IO (2013) Metallic Cu nanoparticles dispersed into porous glass: a simple green chemistry approach to prepare SERS substrates. Mater Lett 108:172–175. https://doi.org/10.1016/j.matlet.2013.06.110

[4] Hering K, Cialla D, Ackermann K et al (2008) SERS: a versatile tool in chemical and biochemical diagnostics. Anal Bioanal Chem 390:113–124. https://doi.org/10.1007/s00216-007-1667-3

[5] Gupta R, Weimer WA (2003) High enhancement factor gold films for surface enhanced Raman spectroscopy. Chem Phys Lett 374:302–306. https://doi.org/10.1016/S0009-2614(03)00737-1

[6] Zhou Z, Lu J, Wang J et al (2020) Trace detection of polycyclic aromatic hydrocarbons in environmental waters by SERS. Spectrochim Acta Part A Mol Biomol Spectrosc 234:118250. https://doi.org/10.1016/j.saa.2020.118250

[7] Liszewska M, Bartosewicz B, Budner B et al (2019) Evaluation of selected SERS substrates for trace detection of explosive materials using portable Raman systems. Vib Spectrosc 100:79–85. https://doi.org/10.1016/j.vibspec.2018.11.002

[8] Fan M, Brolo AG (2009) Silver nanoparticles self-assembly as SERS substrates with near single molecule detection limit. Phys Chem Chem Phys 11:7381. https://doi.org/10.1039/b904744a

[9] Liu H, Zhang L, Lang X et al (2011) Single molecule detection from a large-scale SERS-active Au79Ag21 substrate. Sci Rep 1:112. https://doi.org/10.1038/srep00112

[10] Krajczewski J, Michałowska A, Ctvrtlik R et al (2023) The battle for the future of SERS – TiN vs Au thin films with the same morphology. Appl Surf Sci 618:156703. https://doi.org/10.1016/j.apsusc.2023.156703

[11] Raun A, Saklayen N, Zgrabik C et al (2018) A comparison of inverted and upright laser-activated titanium nitride micropyramids for intracellular delivery. Sci Rep 8:15595. https://doi.org/10.1038/s41598-018-33885-y

[12] Wang X, Wang X, Yue Q et al (2021) Liquid exfoliation of TiN nanodots as novel sonosensitizers for photothermal-enhanced sonodynamic therapy against cancer. Nano Today 39:101170. https://doi.org/10.1016/j.nantod.2021.101170

[13] Zhang B, Wang Z, Zhang C et al (2021) Gold nanocluster-modified titanium nitride for ultrafast photonics applications. Adv Electron Mater 7:2000954. https://doi.org/10.1002/aelm.202000954

[14] Chirumamilla M, Chirumamilla A, Yang Y et al (2017) Large-area ultrabroadband absorber for solar thermophotovoltaics based on 3d titanium nitride nanopillars. Adv Opt Mater 5:1700552. https://doi.org/10.1002/adom.201700552

[15] Barragan AA, Hanukovich S, Bozhilov K et al (2019) Photochemistry of plasmonic titanium nitride nanocrystals. J Phys Chem C 123:21796–21804. https://doi.org/10.1021/acs.jpcc.9b06257

[16] Naldoni A, Guler U, Wang Z et al (2017) Broadband hot-electron collection for solar water splitting with plasmonic titanium nitride. Adv Opt Mater 5:1601031. https://doi.org/10.1002/adom.201601031

[17] Yu M-J, Chang C-L, Lan H-Y et al (2021) Plasmon-enhanced solar-driven hydrogen evolution using titanium nitride metasurface broadband absorbers. ACS Photonics 8:3125–3132. https://doi.org/10.1021/acsphotonics.1c00927

[18] Jen Y-J, Lin M-J, Cheang H-L, Chan T-L (2019) Obliquely deposited titanium nitride nanorod arrays as surface-enhanced raman scattering substrates. Sensors 19:4765. https://doi.org/10.3390/s19214765

[19] Esmaeilzadeh M, Dizajghorbani-Aghdam H, Malekfar R (2021) Surface-Enhanced Raman scattering of methylene blue on titanium nitride nanoparticles synthesized by laser ablation in organic solvents. Spectrochim Acta Part A Mol Biomol Spectrosc 257:119721. https://doi.org/10.1016/j.saa.2021.119721

[20] Kaisar N, Huang Y-T, Jou S et al (2018) Surface-enhanced Raman scattering substrates of flat and wrinkly titanium nitride thin films by sputter deposition. Surf Coatings Technol 337:434–438. https://doi.org/10.1016/j.surfcoat.2018.01.048

[21] Lorite I, Serrano A, Schwartzberg A et al (2013) Surface enhanced Raman spectroscopy by titanium nitride non-continuous thin films. Thin Solid Films 531:144–146. https://doi.org/10.1016/j.tsf.2013.01.024

[22] Soundiraraju B, George BK (2017) Two-dimensional titanium nitride (Ti 2 N) MXene: synthesis, characterization, and potential application as surface-enhanced raman scattering substrate. ACS Nano 11:8892–8900. https://doi.org/10.1021/acsnano.7b03129

[23] Lee S, Sim K, Moon SY et al (2021) Controlled assembly of plasmonic nanoparticles: from static to dynamic nanostructures. Adv Mater 33:2007668. https://doi.org/10.1002/adma.202007668

[24] Rossner C, König TAF, Fery A (2021) Plasmonic properties of colloidal assemblies. Adv Opt Mater 9:2001869. https://doi.org/10.1002/adom.202001869

[25] Gao Z, Shao S, Gao W et al (2021) Morphology-invariant metallic nanoparticles with tunable plasmonic properties. ACS Nano 15:2428–2438. https://doi.org/10.1021/acsnano.0c06123

[26] Yan HH, Zhang Q, Cheng R et al (2021) Size-dependent plasmonic resonance scattering characteristics of gold nanorods for highly sensitive detection of microRNA-27a. ACS Appl Bio Mater 4:3469–3475. https://doi.org/10.1021/acsabm.1c00029

[27] Shinde SL, Ishii S, Dao TD et al (2018) Enhanced solar light absorption and Photoelectrochemical conversion using TiN nanoparticle-incorporated C 3 N 4 –C dot sheets. ACS Appl Mater Interfaces 10:2460–2468. https://doi.org/10.1021/acsami.7b15066

[28] Piao R, Zhang D (2021) Ultra-broadband perfect absorber based on nanoarray of titanium nitride truncated pyramids for solar energy harvesting. Phys E Low-dimensional Syst Nanostructures 134:114829. https://doi.org/10.1016/j.physe.2021.114829

[29] Li L, Lu Y, Qian Z et al (2021) A Ti 2 N MXene-based nanosystem with ultrahigh drug loading for dual-strategy synergistic oncotherapy. Nanoscale 13:18546–18557. https://doi.org/10.1039/D1NR04008A

[30] Wang L, Wang S, Mei L et al (2021) Nanostructures composed of dual plasmonic materials exhibiting high thermal stability and SERS enhancement. Part Part Syst Charact 38:2000321. https://doi.org/10.1002/ppsc.202000321

[31] Hao E, Schatz GC (2004) Electromagnetic fields around silver nanoparticles and dimers. J Chem Phys 120:357–366. https://doi.org/10.1063/1.1629280

[32] Li K, Liu A, Wei D et al (2018) Electromagnetic field redistribution in metal nanoparticle on graphene. Nanoscale Res Lett 13:124. https://doi.org/10.1186/s11671-018-2535-0

[33] Montaño-Priede JL, Pal U (2019) Estimating near electric field of polyhedral gold nanoparticles for plasmon-enhanced spectroscopies. J Phys Chem C 123:11833–11839. https://doi.org/10.1021/acs.jpcc.9b01105

[34] Jiang L, Hassan MM, Ali S et al (2021) Evolving trends in SERS-based techniques for food quality and safety: a review. Trends Food Sci Technol 112:225–240. https://doi.org/10.1016/j.tifs.2021.04.006

[35] Perumal J, Wang Y, Attia ABE et al (2021) Towards a point-of-care SERS sensor for biomedical and agri-food analysis applications: a review of recent advancements. Nanoscale 13:553–580. https://doi.org/10.1039/D0NR06832B

[36] Pavaskar P, Theiss J, Cronin SB (2012) Plasmonic hot spots: nanogap enhancement vs focusing effects from surrounding nanoparticles. Opt Express 20:14656. https://doi.org/10.1364/OE.20.014656

[37] Liu T-Y, Ho J-Y, Wei J-C et al (2014) Label-free and culture-free microbe detection by three dimensional hot-junctions of flexible Raman-enhancing nanohybrid platelets. J Mater Chem B 2:1136–1143. https://doi.org/10.1039/C3TB21469A

[38] Mascaretti L, Barman T, Bricchi BR et al (2021) Controlling the plasmonic properties of titanium nitride thin films by radiofrequency substrate biasing in magnetron sputtering. Appl Surf Sci 554:149543. https://doi.org/10.1016/j.apsusc.2021.149543

[39] Shi H, Zhang H, Chen Z et al (2018) Synthesis of TiN nanostructures by Mg-assisted nitriding TiO$_2$ in N2 for lithium ion storage. Chem Eng J 336:12–19. https://doi.org/10.1016/j.cej.2017.11.036

[40] Park YS, Kodama S, Sekiguchi H (2021) Preparation of metal nitride particles using arc discharge in liquid nitrogen. Nanomaterials 11:2214. https://doi.org/10.3390/nano11092214

[41] Bouaouina B, Mastail C, Besnard A et al (2018) Nanocolumnar TiN thin film growth by oblique angle sputter-deposition: experiments vs. simulations. Mater Des 160:338–349. https://doi.org/10.1016/j.matdes.2018.09.023

[42] Rios MN, Marchese NA, Guido ME (2019) Expression of non-visual opsins opn3 and opn5 in the developing inner retinal cells of birds. Light-responses in müller glial cells. Front Cell Neurosci. https://doi.org/10.3389/fncel.2019.00376

[43] Subr M, Martin P, Peksa V, Kylian O, Hanus J, Prochazka M (2015) Ag nanorod arrays for SERS: aspects of spectral reproducibility, surface contamination, and spectral sensitivity. J Nanomater 5:1–7. https://doi.org/10.1155/2015/729231

[44] Li B, Wang T, Su Q, Wu X, Dong P (2019) Fabrication of Au nanorods by the oblique angle deposition process for trace detection of methamphetamine with surface-enhanced raman scattering. Sensors 19:3742. https://doi.org/10.3390/s19173742

[45] Wu M, Wei H, Wei Y et al (2018) SERS properties of TiN nanotube arrays prepared via reduction nitridation of TiO_2 nanotube arrays derived from anodic oxidation method. Vib Spectrosc 95:32–37. https://doi.org/10.1016/j.vibspec.2018.01.001

[46] Shujun Z, Yue Z, Yujing R, Huiping L, Qian G, Chang G, Yanfeng Z, Wenjie Y, Zhaotan J, Hanchun W, Duan Z, Zhi W (2020) Surface enhanced Raman scattering on ion-beam-deposited TiNx/Si substrates. Nucl. Inst. and Meth. in Phys. Res B 472:24–31. https://doi.org/10.1016/j.nimb.2020.03.008

[47] Le Ru E, Etchegoin P (2009) Principles of Surface-Enhanced Raman Spectroscopy. Elsevier, Amsterdam. https://doi.org/10.1016/B978-0-444-52779-0.00010-6

[48] Patsalas P, Kalfagiannis N, Kassavetis S (2015) Optical properties and plasmonic performance of Titanium Nitride. Materials (Basel) 8:3128–3154. https://doi.org/10.3390/ma8063128

[49] Spengler W, Kaiser R, Bilz H (1975) Resonant Raman scattering in a superconducting transition metal compound–TiN. Solid State Commun 17:19–22. https://doi.org/10.1016/0038-1098(75)90325-7

[50] Spengler W, Kaiser R, Christensen AN, Müller-Vogt G (1978) Raman scattering, superconductivity, and phonon density of states of stoichiometric and nonstoichiometric TiN. Phys Rev B 17:1095–1101. https://doi.org/10.1103/PhysRevB.17.1095

[51] Kudelski A (2003) Structures of monolayers formed from different HS?(CH2)2?X thiols on gold, silver and copper: comparative studies by surface-enhanced Raman scattering. J Raman Spectrosc 34:853–862. https://doi.org/10.1002/jrs.1062

[52] Tian X, Yu Q, Kong X, Zhang M (2022) Preparation of plasmonic Ag@PS composite via seed-mediated in situ growth method and application in SERS. Front Chem. https://doi.org/10.3389/fchem.2022.847203

[53] Moram SSB, Byram C, Soma VR (2020) Gold-nanoparticle- and nanostar-loaded paper-based SERS substrates for sensing nanogram-level Picric acid with a portable Raman spectrometer. Bull Mater Sci 43:53. https://doi.org/10.1007/s12034-019-2017-8

[54] Bai T, Wang M, Cao M et al (2018) Functionalized Au@Ag-Au nanoparticles as an optical and SERS dual probe for lateral flow sensing. Anal Bioanal Chem 410:2291–2303. https://doi.org/10.1007/s00216-018-0850-z